Research Article

Tiantian Wang, Shufeng Yang*, Jingshe Li, Hao Guo, and Zhengyang Chen

Effect of in situ observation of cooling rates on acicular ferrite nucleation

https://doi.org/10.1515/htmp-2022-0026 received February 18, 2022; accepted February 18, 2022

Abstract: The effect of cooling rates on acicular ferrite (AF) nucleation was observed in situ by laser scanning confocal microscopy. The precipitation characteristics of TiN-MnS inclusions, the austenite grain size, and the content and morphologies of AF were analyzed and compared under different cooling rates. The results indicated that with the increase of the cooling rate, the size of TiN-MnS inclusions precipitated in the test steel gradually decreased while the inclusion number increased. When the cooling rate increased from 0.2 to $10^{\circ}\text{C}\cdot\text{s}^{-1}$, the average inclusion size decreased from 2.7 to 1.3 µm. The austenite grain size decreased gradually with the increase of the cooling rate, and the larger the cooling rate was, the more uniform the grain size distribution. The AF proportion increased first and then decreased, it reached the maximum when the cooling rate was 5° C·s⁻¹, which accounted for 82.6%. Meanwhile, the dendrite size decreased gradually, the average length decreased from 30 to 5 µm, and the average width decreased from 2.8 to 0.7 µm when the cooling rate increased from 0.2 to 10°C⋅s⁻¹.

Keywords: cooling rate, *in situ* observation, TiN–MnS inclusions, austenite grains, acicular ferrite

Tiantian Wang, Jingshe Li, Zhengyang Chen: School of Metallurgical and Ecological Engineering, University of Science and Technology Beijing, Beijing 100083, China; Beijing Key Laboratory of Special Melting and Preparation of High-end Metals, Beijing 100083, China Hao Guo: Beijing Key Laboratory of Special Melting and Preparation of High-end Metals, Beijing 100083, China; State Key Laboratory of Advanced Metallurgy, University of Science and Technology Beijing, Beijing 100083, China

1 Introduction

Non-quenched and tempered steel is widely used in major engineering fields such as automobile manufacturing, petrochemical, marine equipment, etc. due to its short manufacturing cycle, energy saving, and excellent mechanical properties [1–3]. In recent years, the production and preparation of non-quenched and tempered steel have become the focus of many engineers and researchers as the steel industry pushes toward the production concept of high efficiency, energy saving, and environmental protection [4].

At present, the microstructural uniformity present in non-quenched and tempered steel affects its service life and performance improvement seriously. Many researchers have dealt with this issue mainly in two ways. Among them, some researchers have improved the microstructure and properties of steel by microalloying [5-7]. Lu et al. [8,9] found that the morphology of MnS inclusions in nonquenched and tempered steel changed to spherical shape gradually through Zr microalloying, and the inclusion distribution was more uniform. In addition, the polygonal ferrite proportion in the grain was increased, the microstructure was refined effectively, and the plasticity of steel was significantly improved. Mirzaee et al. [10] showed that the addition of the Ti element with mass fractions of 0.7 and 1% made the grain size more uniform, reduced the segregation of Cr and C elements, which significantly improved the microstructure of steel. Javaheri et al. [11] demonstrated that the addition of Nb inhibited the growth of austenite grains and refined the grains sufficiently, which made the size distribution more uniform and properties more outstanding.

Other researchers have improved the microstructure of steel by controlling rolling and the cooling rate [12–14]. For example, Bakkaloğlu [15] reduced the rolling temperature from 850 to 740°C and found that the ferrite grain size decreased, the yield strength of the steel increased from 330 to 425 MPa, and the ultimate tensile strength increased from 430 to 528 MPa, the elongation decreased from 38 to 27%. Ghosh et al. [16] found that when the test steel was cooled at the rate of 35°C·s⁻¹, the microstructure

^{*} Corresponding author: Shufeng Yang, School of Metallurgical and Ecological Engineering, University of Science and Technology Beijing, Beijing 100083, China; Beijing Key Laboratory of Special Melting and Preparation of High-end Metals, Beijing 100083, China, e-mail: yangshufeng@ustb.edu.cn

of the steel was mainly acicular ferrite (AF), its strength was 888 MPa, and the elongation was 15.3%. When the rate was 1.15°C·s⁻¹, the major microstructure was pearlite, its strength was decreased, and the ductility was greatly improved. However, when the rate cooling was further decreased, the strength did not change significantly. Bu et al. [17] pointed out that increasing the cooling rate inhibited the precipitation of carbides in Ti-Nb-Mo microalloyed steel, and the average microhardness of ferrite grains was gradually reduced. When the cooling rate was 0.5 and 1°C·s⁻¹, a large number of nanoscale carbides NbC and (Ti, Nb. Mo)C precipitated in the test steel, and the ferrite volume fraction was more than 95%. And the microhardness of the ferrite grains exhibited maxima with a cooling rate of 0.5°C·s⁻¹. When the cooling rate increased to 5°C·s⁻¹, only a few carbides of size less than 20 nm precipitated.

Given the above, many researchers tend to improve the microstructure of steel to improve performance. Nevertheless, microstructure transformation often occurs at high temperature, and the traditional metallographic research method cannot observe the high temperature phase transformation and its cooling microstructure transformation directly. Therefore, in this study, laser scanning confocal microscopy (LSCM) was used to observe the dynamic process of phase transformation *in situ* and study the effect of cooling rates on the precipitation characteristics of AF nucleation site TiN–MnS inclusions and AF nucleation effects, which has an important guiding role in optimizing the controlled cooling process, improving the microstructure and mechanical properties of the steel.

2 Experiments

In this experiment, industrial pure iron, electrolytic manganese, industrial silicon, titanium sponge, and alloys of other elements were used as raw materials. The non-quenched and tempered steel 35 MnVS was melted by a vacuum induction levitation furnace. The chemical composition of the test steel is shown in Table 1.

Cylindrical samples with a size of Φ 7.5 mm \times 3 mm were cut from the test steel. All surfaces of samples were ground to keep bright and prevent the sample oxidation surfaces from affecting the experimental process. One of

the surfaces was polished and treated as the experimental observation surface. The pretreated sample was placed in acetone and ultrasonically cleaned for 10 min and blow-dried. Then, it was put into an alumina crucible while keeping the polished side up. The crucible was placed under a laser scanning confocal microscope to start the experiment. The cooling intensity of different temperature sections was accurately adjusted by a liquid nitrogen cooling system.

Liquidus temperature of the test steel was 1,480°C calculated by the material property software JMatPro. Based on the results, the heating and cooling process of the test steel was designed. The sample was heated from room temperature to 1,500°C with the rate of 130°C·min⁻¹ first, and then the heating rate was reduced to 10°C·min⁻¹. The heating was stopped when the temperature rose to 1,520°C. The cooling of the test steel was carried out according to the cooling scheme established in Table 2. Argon gas was used as the protective gas throughout the experiment with a gas flow rate of 50 mm³·min⁻¹.

3 Results and discussion

3.1 TiN-MnS inclusions

There are many factors affecting the formation of AF, such as austenite grain size, cooling rate, steel

Table 2: Cooling scheme of the test steel in different temperature sections

Cooling section	Temperature range	Cooling rate (°C·s ⁻¹)	Other temperature section cooling rate (°C·s ⁻¹)
Austenitizing temperature section	1,490°C → 950°C	0.2 1.25 5 10	1.25
Phase transition temperature section	950°C → room temperature	0.2 1.25 5 10	1.25

Table 1: Chemical composition of the test steel (wt%)

С	Mn	Si	S	V	N	Al	Ti	Mg	T[0]
0.36	1.29	0.51	0.054	0.10	0.012	0.041	0.025	0.013	0.0122

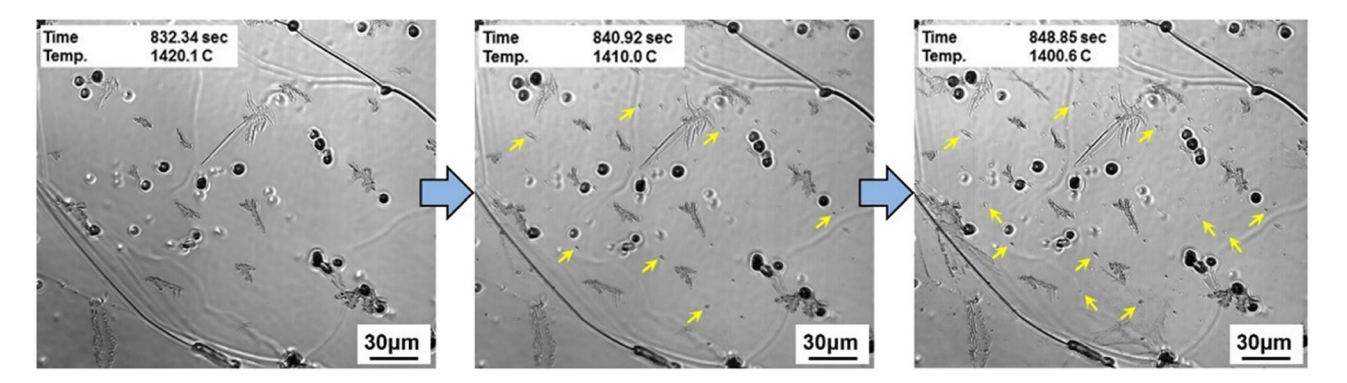


Figure 1: The precipitation process of TiN-MnS inclusions.

composition, inclusions, and so on [18–21]. Research studies have shown that [22] the ability of inclusion-induced AF nucleation depends mainly on its composition and size. TiN–MnS inclusions were one of the main inclusions in the test steel of this study. The distribution of such inclusions was dense and dispersed, which made the induced AF more advantageous in quantity, and thus became the main AF nucleation sites.

Figure 1 shows the precipitation of inclusions observed *in situ* by LSCM. The composition of these inclusions was detected by energy-dispersive spectrometry (EDS) when the

sample was cooled to room temperature. The black spherical inclusions in Figure 1 are primarily composed of Al₂O₃–MgO. These inclusions have a high melting point and maintain solids at molten steel temperature, their composition and content do not change with the increase or decrease of temperature. When the temperature of the test steel dropped to about 1,410°C, a great number of small-sized TiN–MnS inclusions were precipitated in the steel (arrows in Figure 1). These inclusions were dispersed in the steel and the final precipitated TiN–MnS inclusions made no difference under different cooling rates. Figure 2

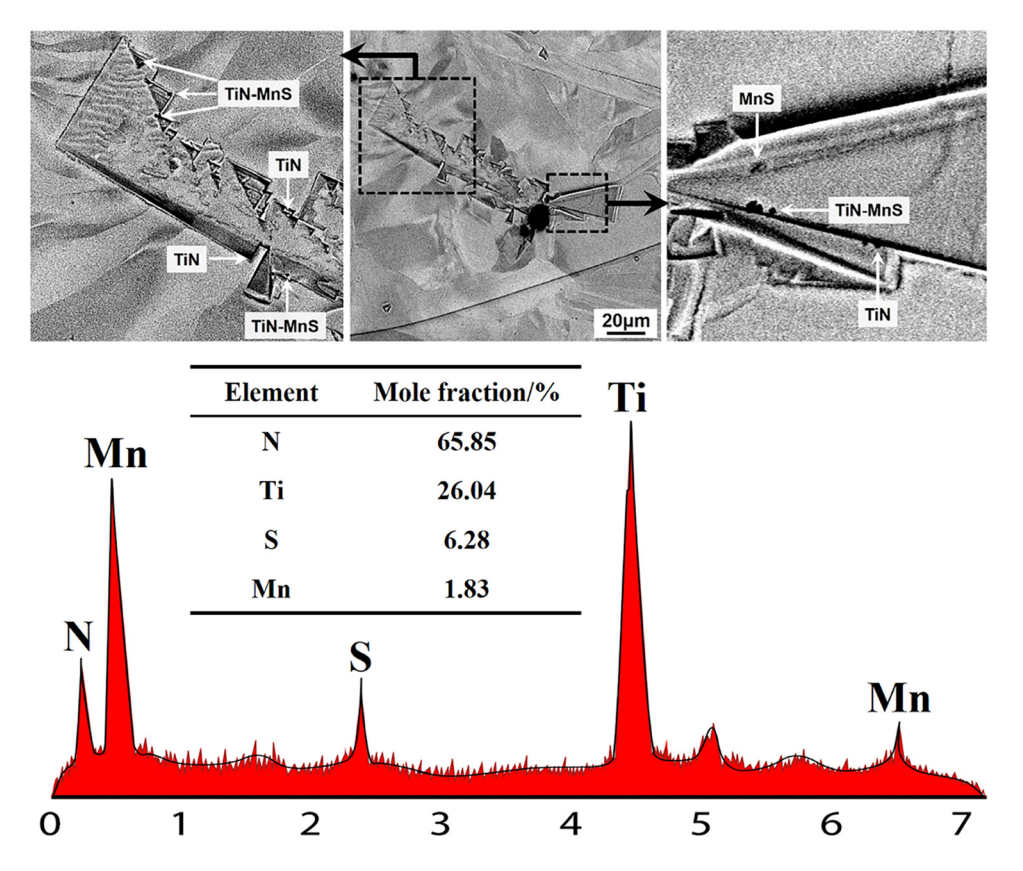


Figure 2: The results of inclusion EDS detection.

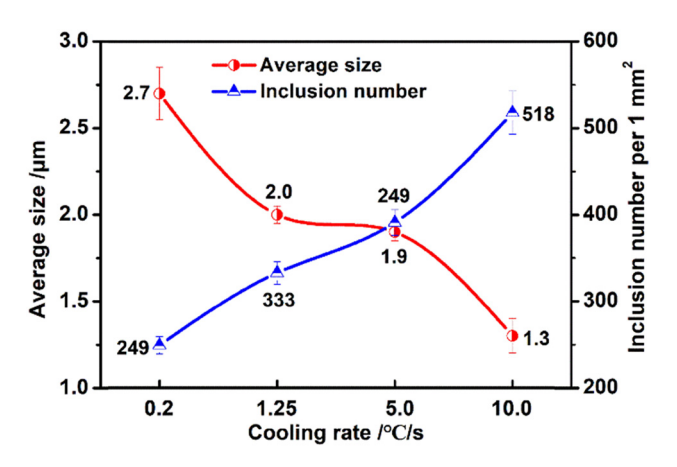


Figure 3: Comparison of the average size and number of TiN-MnS inclusions under different cooling rates.

shows the EDS results of TiN-MnS inclusions. The average size and number of TiN-MnS inclusions precipitated under different cooling rates were measured and counted by Image-Pro Plus. The results are shown in Figure 3.

It could be seen from the statistical results that as the cooling rate increased, the average size of the precipitated TiN-MnS inclusions gradually decreased, while the number gradually increased. When the cooling rate was 0.2°C·s⁻¹, the number of inclusions was 249·mm⁻² and the average size was 2.7 µm. The number of inclusions was doubled and the average size was reduced by 1.4 μ m with the cooling rate increased to 10°C·s⁻¹. As the cooling rate increased, the energy required for inclusion nucleation decreased, and the precipitation was more likely to be promoted. Simultaneously, the time reserved for inclusions from nucleation to growth was shortened, and the inclusions were less likely to collide or grow before they had been precipitated. Therefore, the inclusion size at high cooling rates was relatively small while the inclusion number was large.

Figure 4 shows the process of nucleation and growth of AF on TiN–MnS inclusions observed *in situ* by LSCM.

When the temperature dropped to about 775°C, AF began to nucleate on the inclusions and then continued to grow. When the temperature dropped to 745°C, secondary dendrites appeared on one of the AF dendrites. As the temperature continued to decrease, the number of AF induced by inclusions increased and all of them kept growing in different directions. It could be seen from the figure that AF interlocked with each other. And the AF growth directions were different which was more favorable for forming the self-locking microstructure. Meanwhile, the inclusions were densely and widely distributed and the number of induced AF was also relatively large. The total number of TiN-MnS inclusions in five continuous fields of view and the number of inclusions that could be used as AF nucleation sites were statistically analyzed. The results indicated that approximately 75.0% TiN-MnS inclusions could induce AF well.

3.2 Austenite grain size

According to the Hall-Petch relationship, the finer the grain is, the higher is the strength [23]. The grain size of the metal material at room temperature is related to the austenite grain size [24,25]. It is well known that the smaller the austenite grain size is, the smaller is the grain size of the transformation product, so it has some influence on the microstructure and properties of the steel. Many scholars [20,26-28] believe that the AF content in steel has a great relationship with the austenite grain size. There is a range of austenite grain size, within which the number and size of AF generated reach the optimal balance. When the grain size is outside this range, the proportion of AF decreases. Studies have shown that [28,29] the austenite grain size is not only related to the steel composition, heating rate, holding time, etc. but also related to the cooling rate of molten steel.

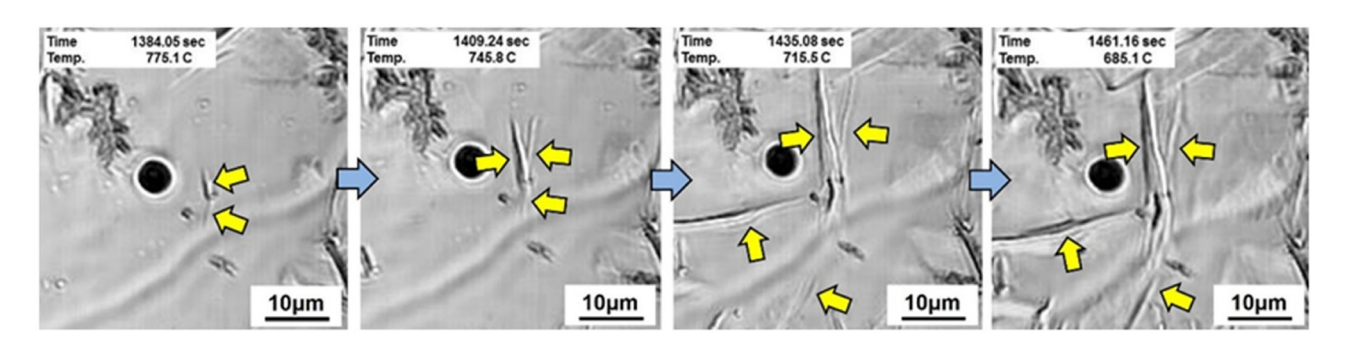


Figure 4: AF nucleates on TiN-MnS inclusions.

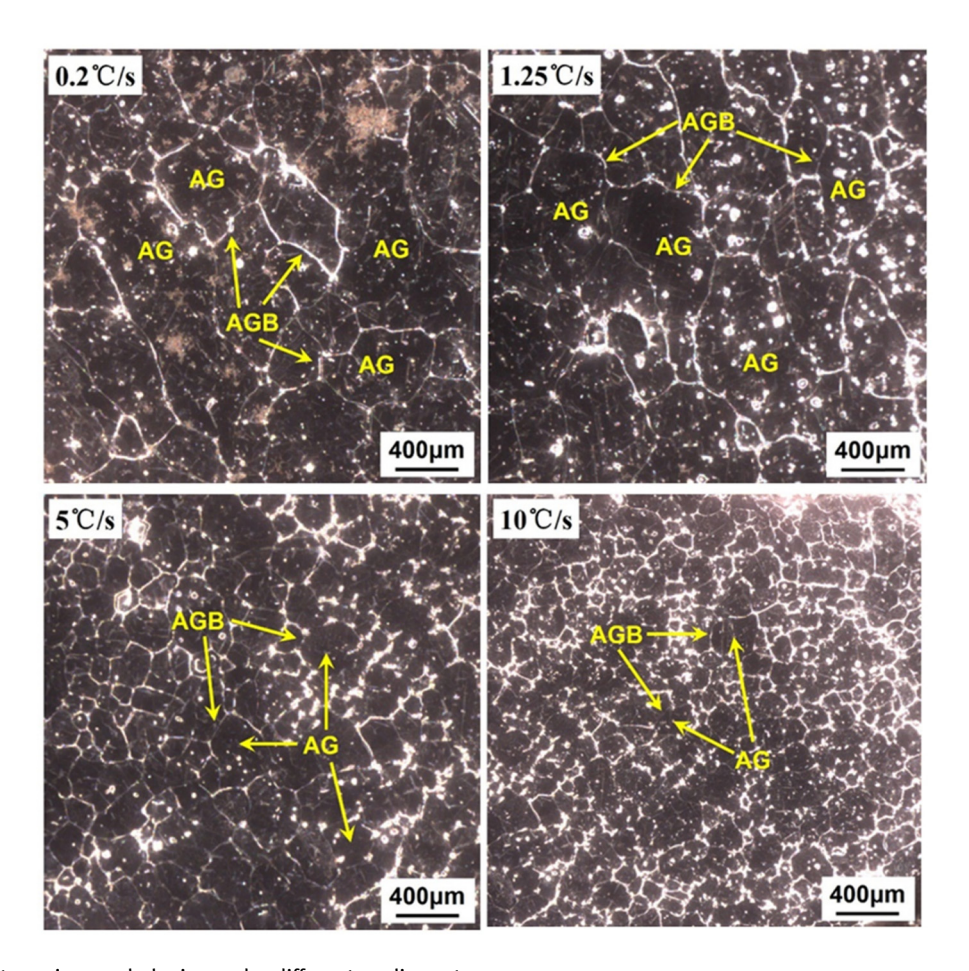


Figure 5: Austenite grain morphologies under different cooling rates.

Figure 5 shows the morphologies of austenite grains under different rates observed by scanning electron microscopy. AG in the figure represents austenite grain and AGB represents austenite grain boundary. On the whole, the austenite grain size gradually decreased with the increase of the

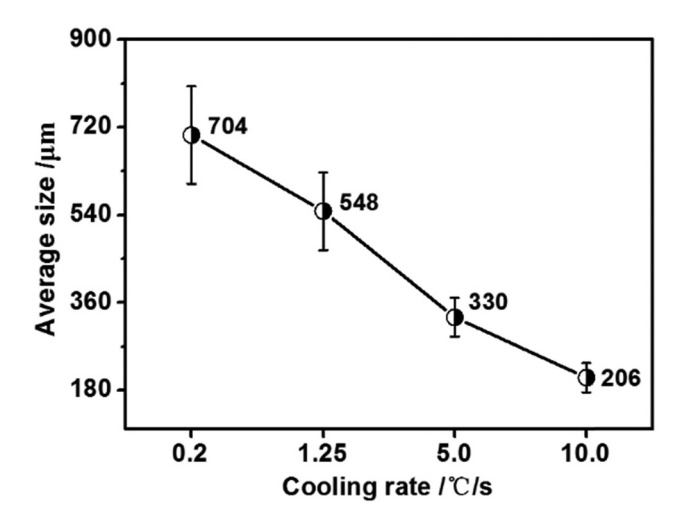


Figure 6: Austenite grain average size under different cooling rates.

cooling rate. This was due to the high cooling rate of steel, which decreased the time left for the austenite grain boundary migration and the austenite grain growth, making it too late for the grains to grow. The statistical results of austenite grain average size are shown in Figure 6. It could be found that as the cooling rate increased from 0.2 to 1.25, 5, and 10°C·s⁻¹, respectively, the austenite grain average size decreased by 22.2, 53.1, and 70.7%. And the larger the cooling rate was, the more uniformly the austenite grain size was distributed. The difference between the maximum and minimum grain size was only about 30 μm when the cooling rate was 10°C·s⁻¹, while the difference could reach about 100 μm when the cooling rates were 0.2 and 1.25°C·s⁻¹.

3.3 AF morphology

The size of austenite grains is an important factor affecting the nucleation effect of AF. Lee and Pan [30] showed that the critical austenite grain size of AF formed in titanium-killed steel was $50 \, \mu m$. As the austenite grain size increased,

186 — Tiantian Wang et al. DE GRUYTER

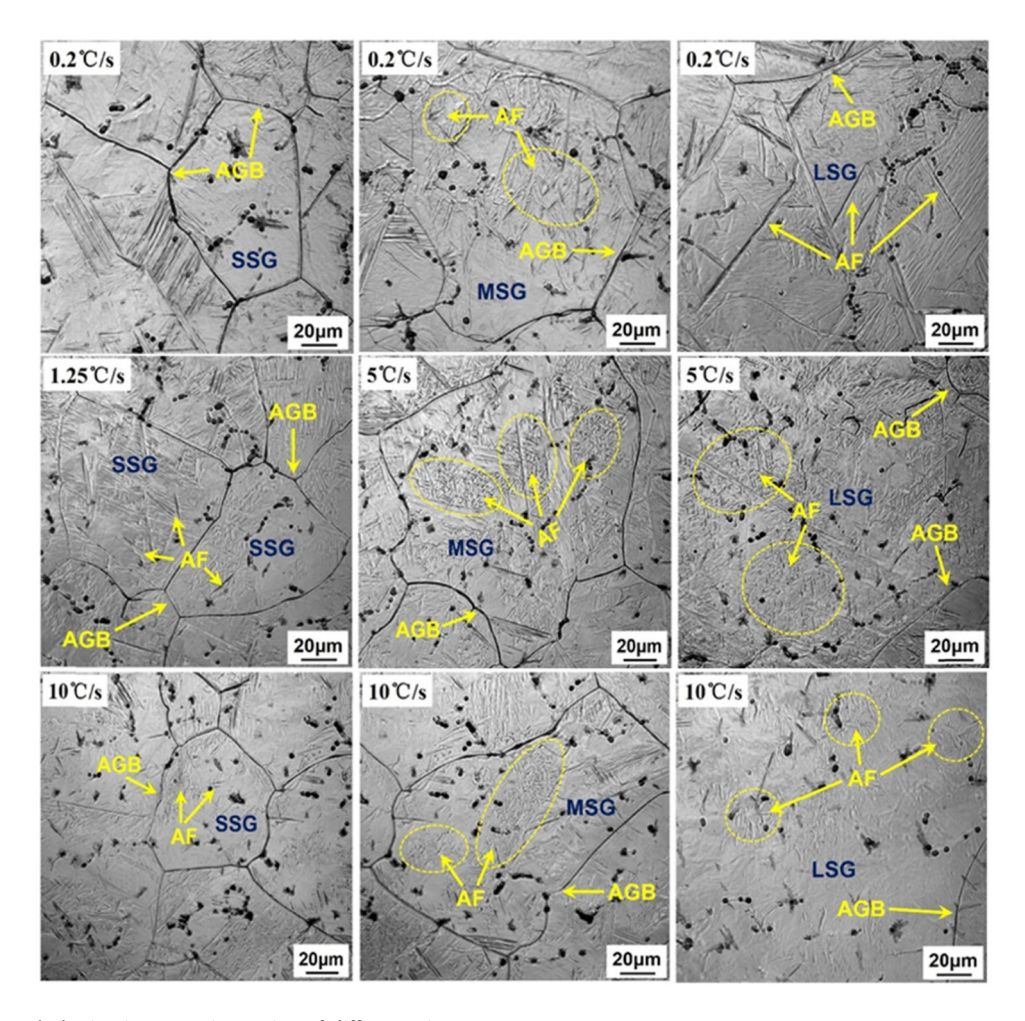


Figure 7: AF morphologies in austenite grains of different sizes.

the ability of AF nucleation increased and it began to decrease after reaching a maximum value (180 to 190 μm). Wan et al. [31] observed a critical austenite grain size of AF formed in Zr–Ti compound-deoxidized steel of 55 μm in situ by LSCM. Thewlis [32] carried out a lot of experimental studies, indicating that the intragranular AF content could be maximized when the austenite grain size reached 140 μm . Barbaro et al. [33] believed that more AF could be obtained when the austenite grain size exceeded 110 μm . Therefore, in this study, the critical austenite grain size of forming AF and the maximum AF content were taken as the demarcation point, the austenite grains were divided into small-sized grains, medium-sized grains, and large-sized grains.

Figure 7 shows the AF morphologies in austenite grains of different sizes. SSG in the figure represents small-sized austenite grain, MSG represents medium-sized grain, and LSG represents large-sized austenite grains. Comparing the morphological characteristics of AF under different cooling rates in Figure 7, it was pointed that there was a common phenomenon in the microstructure

morphologies under different cooling rates. As the austenite grain size increased from small to large, the number of AF in the grains increased first and then decreased. This is

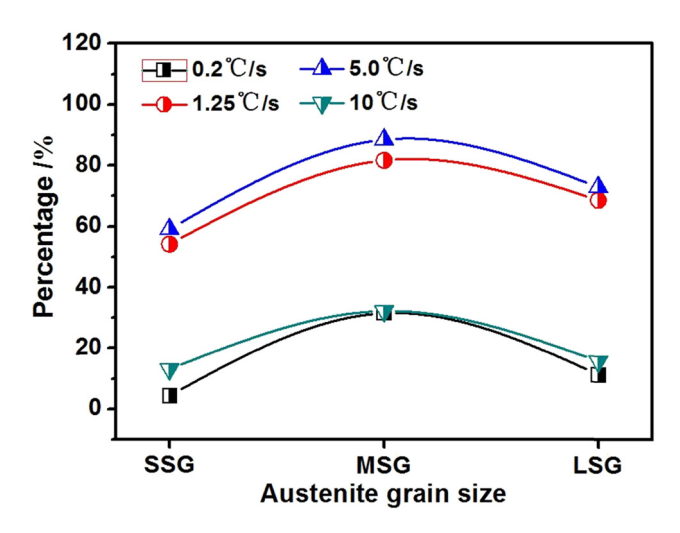


Figure 8: AF proportion in austenite grains of different sizes.

to say, the number and proportion of AF in the mediumsized austenite grains were relatively large, small in smallsized austenite grains relatively, while those of large-sized austenite grains were between them.

The statistical results of the AF proportion in austenite grains of different sizes under different cooling rates are shown in Figure 8. The results indicated that with the cooling rate increased, the AF proportion in the austenite grains increased first and then decreased. The proportion was the smallest when the cooling rate was $0.2^{\circ}\text{C}\cdot\text{s}^{-1}$, and the proportion reached the maximum when the cooling rate was $5^{\circ}\text{C}\cdot\text{s}^{-1}$. At the four kinds of cooling rates, the AF content in medium-sized austenite grains was the highest and that in the small-sized austenite grains was the lowest. This confirmed that the austenite grain size and the cooling rate affected the AF content of the austenite grains to some extent.

The cooling rate not only affects the AF content in the austenite grains but also affects the morphologies. Figure 9 shows the AF morphologies of the test steel under different cooling rates observed by LSCM. When the cooling rate was 0.2°C·s⁻¹, the AF structure was obliquely crossed and the self-locking property was good but the distribution was relatively scattered. When the cooling rate increased to 1.25°C·s⁻¹ and 5°C·s⁻¹, the AF was crisscrossed with good

self-locking properties as the number in the austenite grains was obviously increased and the distribution was uniform and dense. The number and density of AF were decreased and the microstructure distribution was scattered with the cooling rate increased to 10°C·s⁻¹. Simultaneously, it could be seen from the figure that as the cooling rate continued to increase, the size of AF decreased gradually.

The size of AF in the test steel under different cooling rates was measured, and the proportion of AF was counted. The results are shown in Figure 10. The results indicated that the average length and width of AF dendrites in the test steel gradually decreased with the increase of the cooling rate. At a cooling rate of 0.2°C·s⁻¹, the dendrite average length was 30 µm and the average width was 2.8 µm, which was significantly larger than the dendrite size at other cooling rates. When the cooling rate was 10°C·s⁻¹, the dendrite size was the smallest, the average length was only 5 μm, and the average width was 0.7 μm. And the difference of the dendrite average length between these two cooling rates was 25 µm. Figure 10(b) shows the statistical result of the AF proportion under different cooling rates. With the cooling rate increased, the AF proportion increased first and then decreased. When the cooling rate was 0.2°C·s⁻¹, the AF proportion was the smallest, only 13.1%. When the cooling

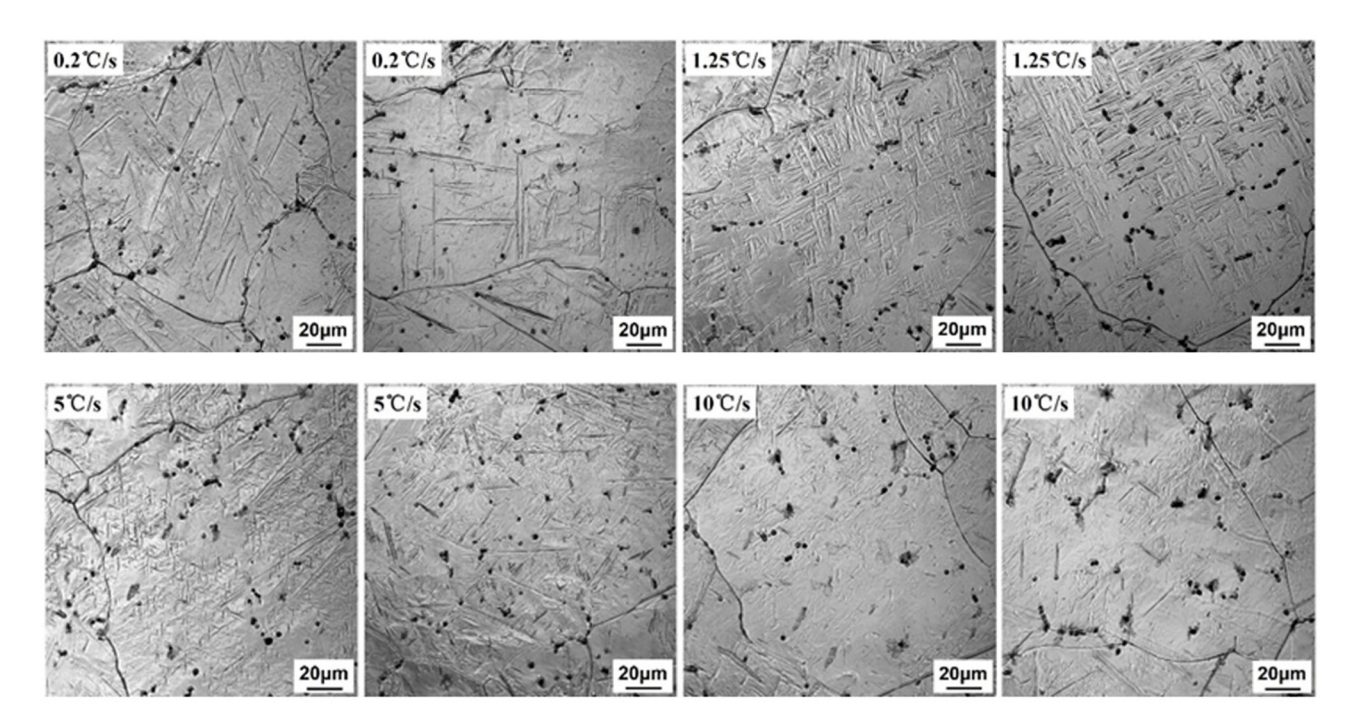


Figure 9: AF morphologies under different cooling rates.

188 — Tiantian Wang et al. DE GRUYTER

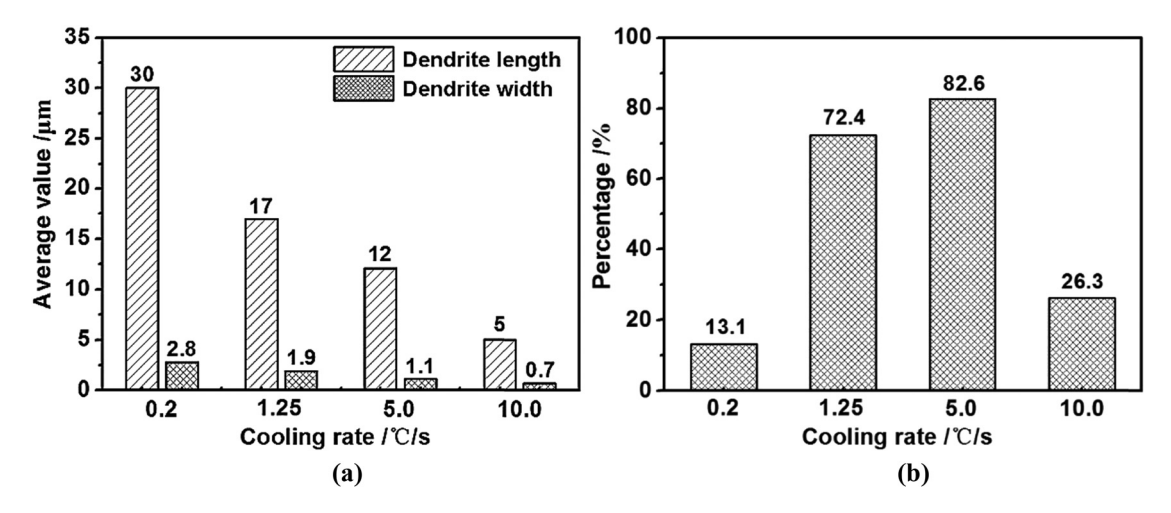


Figure 10: Comparison of AF dendrite size and proportion under different cooling rates. (a) AF dendrites size; (b) AF proportion.

rate increased to 5°C·s⁻¹, the proportion reached the maximum, 82.6%, and the difference between them was about 69.5%. The results were consistent with the statistical results of Figure 8.

The cooling rate has an important influence on the microstructure of the steel. Kang et al. [34] investigated the microstructural evolution of high strength low alloy steel under the continuous cooling rates of 1-50°C·s⁻¹ and found that AF formed at the cooling rate of 10-30°C·s⁻¹. Granular bainite would be formed if the cooling rate was too low while lath-type bainite was dominant when the cooling rate was high. Mun et al. [35] showed that when the cooling rate was 1–5°C·s⁻¹, the microstructure of the test steel was mainly polygonal ferrite. When the cooling rate increased, the ferrite microstructure in the steel became refined and the AF volume fraction increased. The essence of austenite phase transformation is that the carbon atoms in the austenite region are diffused by heating [36]. When the cooling rate is low, the carbon atoms have enough time to diffuse, which will result in the finer ferrite grains previously formed coarse. Then, the adjacent ferritic structure fuses with each other, making the structure coarse again and eventually forming massive granular ferrites. Similarly, granular ferrites will fuse with each other and become larger. Thus, when the cooling rate is low, AF takes a small proportion in the microstructure.

In addition, the decrease of molten steel temperature provides a driving force for austenite phase transformation, which is mainly driven by the degree of undercooling coming from the molten steel [37]. The speed of the cooling rate reflects the degree of undercooling in unit time to some extent. The higher the cooling rate is, the greater is the degree of undercooling of molten steel. The high degree of under cooling will promote the driving

force of austenite phase transformation and the precipitation of ferrites. However, when the cooling rate is too high, the degree of under cooling of the molten steel is too large, so the austenite grains are too late to grow and the carbon content inside the grains concentrates, which inhibits the AF nucleation and decrease the AF proportion in the microstructure. Therefore, as the cooling rate increases, the proportion of AF increases first and then decreases.

4 Conclusions

The microstructure uniformity of the steel has a great impact on the improvement of its service life and performance. Therefore, this study improved the microstructure of steel by controlling the cooling rate to improve its performance. Based on the traditional metallographic research method, it is impossible to directly observe the high temperature phase transformation and its cooling microstructure transformation. LSCM was used to observe the dynamic process of phase transformation in situ and study the effect of the cooling rate on the precipitation characteristics of AF nucleation site TiN-MnS inclusions and the AF nucleation effect. Thus, it provided engineering guidance and theoretical basis for optimizing the cooling process and selecting reasonable cooling rates to improve the microstructure and mechanical properties of steel. The following conclusions could be drawn from this study:

(1) In this study, as the cooling rate increased, the size of TiN-MnS inclusions precipitated in the test steel gradually decreased while the number gradually increased. The average size reduced from 2.7 to 1.3 µm while the

- number increased from 249 to 518 mm⁻² with the cooling rate increasing from 0.2 to $10^{\circ}\text{C}\cdot\text{s}^{-1}$.
- (2) When the cooling rate increased from 0.2 to 1.25, 5, and 10°C·s⁻¹, the average austenite grain size in steel decreased by 22.2, 53.1, and 70.7%, respectively. And the larger the cooling rate was, the more uniform the grain size distribution.
- (3) As the cooling rate increased, the AF proportion in the test steel increased first and then decreased while the dendrite size gradually decreased. When the cooling rate was 5°C·s⁻¹, the proportion reached the maximum, 82.6%. The dendrite average length decreased from 30 to 5 µm while the average width decreased from 2.8 to 0.7 µm with the cooling rate increasing from 0.2 to 10°C⋅s⁻¹.

Acknowledgments: The authors gratefully acknowledge the support by the National Natural Science Foundation of China (NSFC, Nos. 51734023 and 51734003).

Funding information: This work was financially supported by the National Natural Science Foundation of China (Great Nos. 51674023 and 51734003).

Author contributions: Tiantian Wang performed the experiments, analyzed the data and wrote the manuscript with help from all the other authors; Shufeng Yang and Jingshe Li helped to perform the analysis with constructive discussions, conceived the work and supervised the whole project; Hao Guo and Zhengyang Chen clarified the logic of the manuscript and revised it.

Conflict of interest: The authors declare no conflict of interest.

Data availability statement: The data used to support the findings of this study cannot be shared at this time as the data also forms part of an ongoing study.

References

- Lu, J. L., G. G. Cheng, J. L. Che, L. S. Wang, and G. J. Xiong. Flotation mechanisms of molybdenite fines by neutral oils. Metals and Materials International, Vol. 25, 2018, pp. 1-14.
- Hui, W. J., Y. J. Zhang, C. W. Shao, S. L. Chen, X. L. Zhao, and H. Dong. Microstructural effects on high-cycle fatigue properties of microalloyed medium carbon steel 38MnVS. Materials Science and Engineering: A, Vol. 640, 2015, pp. 147-153.
- [3] Cao, J., J. Yan, J. Zhang, and T. G. Yu. High molecular weight βpoly(L-malic acid) produced by A. pullulans with Ca2+ added

- repeated batch culture. Materials Science and Engineering: A, Vol. 639, 2015, pp. 192-197.
- Zhou, B., Y. Shen, L. Tan, H. X. Yang, W. Q. Cao, and Y. Z. Bao. [4] Research on a New Process of the Non-quenched and Tempered Steel with High Strength and High Toughness. Physics Procedia, Vol. 50, 2013, pp. 25-31.
- Zou, X. D., J. C. Sun, D. P. Zhao, H. Matsuura, and C. Wang. Effects of Zr addition on evolution behavior of inclusions in EH36 shipbuilding steel: from casting to welding. Journal of Iron and Steel Research International, Vol. 25, 2018, pp. 164-172.
- Sasidhar, K. N., T. Dhande, N. Javed, A. Ghosh, M. Mukherjee, V. Sharma, et al. Effect of transformation texture on the impact toughness of hot-rolled Ti + Nb microalloyed steel. Material Design, Vol. 128, 2017, pp. 86-97.
- [7] Hu, J., L. X. Du, M. Zang, S. J. Yin, Y. G. Wang, X. Y. Qi, et al. On the determining role of acicular ferrite in V-N microalloyed steel in increasing strength-toughness combination. Materials Characterization, Vol. 118, 2016, pp. 446-453.
- Lu, J. L., G. G. Cheng, B. Tan, and J. L. Che. ISUP Group 4 a Homogenous Group of Prostate Cancers? ISIJ International, Vol. 58, 2018, pp. 921-928.
- [9] Lu, J. L., G. G. Cheng, L. Chen, J. L. Che, G. J. Xiong, and L. S. Wang. Distribution and Morphology of MnS Inclusions in Resulfurized Non-Quenched and Tempered Steel with Zr Addition. ISIJ International, Vol. 58, 2018, pp. 1307-1315.
- Mirzaee, M., A. Momeni, H. Keshmiri, and R. Razavinejad. Effect of Titanium and Niobium on Modifying the Microstructure of Cast K100 Tool Steel. Metallurgical and Materials Transactions B, Vol. 45, 2014, pp. 2304-2314.
- Javaheri, V., N. Khodaie, A. Kaijalainen, and D. Porter. Effect of niobium and phase transformation temperature on the microstructure and texture of a novel 0.40% C thermomechanically processed steel. Materials Characterization, Vol. 142, 2018, pp. 295-308.
- [12] Karmakar, A., P. Sahu, S. Neogy, D. Chakrabarti, R. Mitra, S. Mukherjee, et al. Effect of Cooling Rate and Chemical Composition on Microstructure and Properties of Naturally Cooled Vanadium-Microalloyed Steels. Metallurgical and Materials Transactions A, Vol. 48, 2017, pp. 1581-1595.
- [13] Kaijalainen, A. J., M. Liimatainen, V. Kesti, J. Heikkala, T. Liimatainen, and D. Porter. Influence of Composition and Hot Rolling on the Subsurface Microstructure and Bendability of Ultrahigh-Strength Strip. Metallurgical and Materials Transactions A, Vol. 47, 2016, pp. 4175-4188.
- [14] Ceschini, L., A. Marconi, C. Martini, A. Morri, and A. D. Schino. Tensile and impact behaviour of a microalloyed medium carbon steel: Effect of the cooling condition and corresponding microstructure. Material Design, Vol. 45, 2013, pp. 171-178.
- Bakkaloğlu, A. Effect of processing parameters on the microstructure and properties of an Nb microalloyed steel. Materials Letters, Vol. 56, 2002, pp. 200-209.
- Ghosh, A., S. Das, S. Chatterjee, and P. Ramachandra Rao. Effect of cooling rate on structure and properties of an ultralow carbon HSLA-100 grade steel. Materials Characterization, Vol. 56, 2006, pp. 59-65.
- [17] Bu, F. Z., X. M. Wang, L. Chen, S. W. Yang, C. J. Shang, and R. D. K. Misra. The molecular origins of twist in cellulose I-beta. Materials Characterization, Vol. 102, 2015, pp. 146-155.

- [18] Sarma, D. S., A. V. Karasev, and P. G. Jönsson. On the Role of Non-metallic Inclusions in the Nucleation of Acicular Ferrite in Steels. *ISIJ International*, Vol. 49, 2009, pp. 1063–1074.
- [19] Zhao, F., M. Wu, B. Jiang, C. L. Zhang, J. X. Xie, and Y. Z. Liu. The effect of carbon contents on intragranular ferrite formed in the V-Ti-N microalloyed steel with a carbon content gradient prepared by controlling the surface decarburization. *Materials Characterization*, Vol. 140, 2018, pp. 217–224.
- [20] Zhang, D., H. Terasaki, and Y. I. Komizo. Structures and energies of the radicals and anions generated from chlorpyrifos. Acta Materialia, Vol. 58, 2010, pp. 1369–1378.
- [21] Cheng, L., C. Xu, L. Lu, L. Yu, and K. M. Wu. Experimental and first principle calculation study on titanium, zirconium and aluminum oxides in promoting ferrite nucleation. *Journal of Alloys and Compounds*, Vol. 742, 2018, pp. 112–122.
- [22] Loder, D., S. K. Michelic, A. Mayerhofer, and C. Bernhard. On the Capability of Nonmetallic Inclusions to Act as Nuclei for Acicular Ferrite in Different Steel Grades. *Metallurgical and Materials Transactions B*, Vol. 48, 2017, pp. 1–15.
- [23] Chokshi, A. H., A. Rosen, J. Karch, and H. Gleiter. On the validity of the hall-petch relationship in nanocrystalline materials. *Scripta Metallurgica*, Vol. 23, 1989, pp. 1679–1683.
- [24] Elwazri, A. M., S. Yue, and P. Wanjara. Effect of prior-austenite grain size and transformation temperature on nodule size of microalloyed hypereutectoid steels. *Metallurgical* and Materials Transactions B, Vol. 36, 2005, pp. 2297–2305.
- [25] Khlusova, E. I., A. A. Kruglova, and V. V. Orlov. Effect of chemical composition and heat and strain treatment on austenite grain size in low-carbon steel. *Metal Science and Heat Treatment*, Vol. 49, 2007, pp. 549–555.
- [26] Farrar, R. A., Z. Zhang, S. R. Bannister, and G. S. Barritte. The effect of prior austenite grain size on the transformation behaviour of C-Mn-Ni weld metal. *Journal of Materials Science*, Vol. 28, 1993, pp. 1385–1390.

- [27] Lee, J. L. and Y. T. Pan. The Formation of Intragranular Acicular Ferrite in Simulated Heat-affected Zone. *ISIJ International*, Vol. 35, 1995, pp. 1027–1033.
- [28] Maropoulos, S., S. Karagiannis, and N. Ridley. Factors affecting prior austenite grain size in low alloy steel. *Journal of Materials Science*, Vol. 42, 2007, pp. 1309–1320.
- [29] Kim, H. S., Y. Kobayashi, S. Tsukamoto, and K. Nagai. Effect of cooling rate on microstructure evolution of rapidly cooled high-impurity steels. *Materials Science and Engineering: A*, Vol. 403, 2005, pp. 311–317.
- [30] Lee, J. L. and Y. T. Pan. Purification and properties of branchedchain alpha-keto acid dehydrogenase kinase from bovine kidney. *Materials Science and Engineering: A*, Vol. 136, 1991, pp. 109–119.
- [31] Wan, X. L., K. M. Wu, L. Cheng, and R. Wei. *In-situ* Observations of Acicular Ferrite Growth Behavior in the Simulated Coarsegrained Heat-affected Zone of High-strength Low-alloy Steels. *ISIJ International*, Vol. 55, 2015, pp. 679–685.
- [32] Thewlis, G. Transformation kinetics of ferrous weld metals.

 Materials Science and Technology, Vol. 10, 1994, pp. 110–125.
- [33] Barbaro, F. J., P. Krauklis, and K. E. Easterling. Formation of acicular ferrite at oxide particles in steels. *Materials Science* and Technology, Vol. 5, 1989, pp. 1057–1068.
- [34] Kang, J. S., J. B. Seol, and C. G. Park. MicroRNA-21 regulates stemness in cancer cells. *Materials Characterization*, Vol. 79, 2013, pp. 110–121.
- [35] Mun, D. J., E. J. Shin, Y. W. Choi, J. S. Lee, and Y. M. Koo. Effects of cooling rate, austenitizing temperature and austenite deformation on the transformation behavior of high-strength boron steel. *Materials Science and Engineering: A*, Vol. 545, 2012, pp. 214–224.
- [36] Erdogan, M. Effect of austenite dispersion on phase transformation in dual phase steel. *Scripta Materialia*, Vol. 48, 2003, pp. 501–506.
- [37] Gamsjäger, E., J. Svoboda, and F. D. Fischera. Austenite-to-ferrite phase transformation in low-alloyed steels. *Computational Materials Science*, Vol. 32, 2005, pp. 360–369.